

Article

Reduction of Trinitrobenzene to Amines with Molecular Hydrogen over Chrysocolla-like Catalysts

Olga A. Kirichenko , Elena V. Shuvalova , Gennady I. Kapustin, Nikolay A. Davshan , Igor V. Mishin and Leonid M. Kustov *

Zelinsky Institute of Organic Chemistry, Russian Academy of Sciences, Leninsky Prospekt 47, Moscow 119991, Russia; evshouvalova@yandex.ru (E.V.S.)

* Correspondence: lmkustov@mail.ru

Abstract: The cheap non-noble Cu–SiO₂-based nanocatalysts are under intensive study in different reactions resulting in useful chemicals, yet their application in environment protection is poorly studied. In the present work, the influence of the Cu loading (3–15 wt%) on the catalytic behavior of Cu/SiO₂ materials was first precisely studied in the hydrogenation of hazardous trinitrobenzene to valuable aromatic amines with molecular hydrogen. The catalysts have been synthesized by the method of deposition–precipitation using urea. The catalyst characterization by XRD, TPR-H₂, SEM, TEM, and N₂ adsorption methods confirmed that they include nanoparticles of the micro-mesoporous chrysocolla-like phase supported in the mesopores of a commercial SiO₂ carrier, as well as revealed formation of the highly dispersed CuO phase in the sample with the highest Cu loading. Variation in reaction conditions showed the optimal ones (170 °C, 1.3 MPa H₂) resulting in complete trinitrobenzene conversion with a triaminobenzene yield of 65% for the catalyst with a 15% Cu loading, and the best yield of 82% was obtained over the catalyst with 10% Cu calcined at 600 °C. The results show the potential of Cu phyllosilicate-based catalysts for the utilization of trinitroaromatic compounds via catalytic hydrogenation to amines and their possible applications in a remediation treatment system.

Keywords: copper phyllosilicate catalysts; nitroarene hydrogenation; trinitrobenzene



Citation: Kirichenko, O.A.; Shuvalova, E.V.; Kapustin, G.I.; Davshan, N.A.; Mishin, I.V.; Kustov, L.M. Reduction of Trinitrobenzene to Amines with Molecular Hydrogen over Chrysocolla-like Catalysts. *Catalysts* **2024**, *14*, 686. <https://doi.org/10.3390/catal14100686>

Academic Editors: Ulises Sedran and Mohammad Mozahar Hossain

Received: 24 July 2024

Revised: 11 August 2024

Accepted: 30 September 2024

Published: 2 October 2024



Copyright: © 2024 by the authors. Licensee MDPI, Basel, Switzerland. This article is an open access article distributed under the terms and conditions of the Creative Commons Attribution (CC BY) license (<https://creativecommons.org/licenses/by/4.0/>).

1. Introduction

In the past 10 years, the development of novel Cu-based catalysts has received wide acceptance in the catalytic synthesis of platform chemicals including well-known processes [1–6], as well as in new processes based on renewable raw sources, especially selective hydrogenation with molecular hydrogen (synthesis of valuable alcohols, furanic fuels, and amines) [7–19].

The selective catalytic reduction in nitroarenes (SCRN) to the corresponding anilines, which are valuable intermediates and chemicals in a number of industrial fields, has attracted much attention [18–23]. Growing interest has been paid to SCRN applications in environment protection because nitroarenes possess various hazardous effects on human health and the environment, and they are constituents of harmful waste and pollutant stocks in industrial production [24–29]. Precious metal catalysts (PMCs) exhibit high activity in SCRN, and their selectivity in reduction in nitro groups can be increased with PMC modified with transition metal compounds [19–21,30–33]. The growing PM prices and limited resources increase the costs of catalysts and chemicals produced, as well as the expenditures for environment protection processes and technologies.

Today, non-precious metals are being considered for their application in the catalytic hydrogenation of nitroarenes instead of PMCs due to their abundance and low price [18–20,34–39]. Cu-based catalysts possess better stability and safety compared to Co and Ni catalysts, and are more active than Fe catalysts. Supported Cu catalysts have

been preferably used in nitroarene reduction by transfer hydrogenation using hydrogen donors ($\text{NH}_3\text{-BH}_3$ [40,41], NaBH_4 [21,33,42–46], $\text{N}_2\text{H}_4\text{H}_2\text{O}$ [47], and 2-butanol [48]) rather than in direct hydrogenation with molecular H_2 . However, the application of NaBH_4 and $\text{NH}_3\text{-BH}_3$ as reducing agents results in the formation of large amounts of solid wastes and contaminated organic and aqueous stocks. $\text{N}_2\text{H}_4\text{H}_2\text{O}$ -mediated reduction is much cleaner, as the only byproducts are gaseous N_2 and H_2 , yet the high selectivity may be difficult to achieve in the presence of a carbon–carbon double bond, triple bond, and aldehyde [21,47]. The major advantage of molecular H_2 is its recognition as a “green” hydrogen source for the selective reduction in nitrobenzenes because of the formation of water as the only byproduct. Molecular H_2 is the last in the selectivity sequence for diverse hydrogen sources, yet it is cheap and commercially produced on a large scale.

Formation of oxygen vacancies on the surface of CuO (111) in the reducing environment was shown to facilitate stronger nitrobenzene binding and reduced the activation barrier for N-O dissociation [47]. Moreover, it was claimed that the adsorption and dissociation of molecular hydrogen can occur at the $\text{Cu}^{n+}\text{-O-SiO}_x$ interface or on the SiO_2 surface [9,43] in Cu phyllosilicate catalysts. Both of these facts and the results regarding the successful reduction of nitro groups to amino groups in nitroarenes with molecular H_2 on Cu catalysts [18,19,49] demonstrate a possible way for the reduction of different nitroarenes with molecular H_2 . Cu/SiO_2 catalysts provide the possibility of hydrogenation of nitroarenes at a lower hydrogen pressure (1.5 MPa) [50,51] than CuO supported on other oxides (4 MPa) [49].

Trinitroaromatic compounds are highly toxic [24,52]. Their environmental transformation products are equally or more toxic as the parent nitroaromatic molecules [53]. To remediate areas contaminated with these compounds, the following technologies have been applied and are still under study: bioremediation, common remediation treatment, adsorption, advanced oxidation processes, and chemical reduction [54–60]. Chemical reduction supposes catalytic hydrogenation of nitro compounds to corresponding amines, and therefore, alone it is not a complete remediation process because the formed amines are toxic and must be treated further. The oxidative polymerization, which causes amines to bind into polymers, and biological transformation have been proposed for further treatment. However, from our viewpoint, the further utilization of amines as chemicals for commercial use [61] looks more promising, especially if one combines the chemical reduction process with adsorption technology.

Hydrogenation of aromatic trinitro compounds is far less studied than hydrogenation of mono and dinitro aromatic compounds; nevertheless, it is found to proceed in an organic solvent medium at an elevated hydrogen pressure and is catalyzed by Raney Ni , PtO_2 , as well as Ni , Pd , Pt , Ru , Rh , and polymetallic compositions deposited on activated carbon, SiO_2 , Al_2O_3 , zeolites, or other supports [62–65]. 2,4,6-Trinitrobenzoic acid was selectively hydrogenated even in the aqueous phase over a Pd/C catalyst to produce triaminobenzene or to non-aromatic cyclohexane-1,3,5-trione trioxime [66,67]. The prices of PMC are too high for implementation in the industrial or waste treatment technologies; moreover, Pd dissolves in the presence of nitroaromatics [68,69]. Recently, it was shown that Cu -based materials possess a high catalytic activity and selectivity in hydrogenation of aromatic trinitro compounds to corresponding amines [70,71]. Hydrogenation of 1,3,5-trinitrobenzene (TNB) in a flow reactor over the supported 21% $\text{CuO/Al}_2\text{O}_3$ catalyst at 120 °C, total pressure of 30 bar, and methanol as a solvent resulted in about a 68% yield as sulfuric acid double salt of 1,3,5-triaminobenzene (TAB) [70]. The application of Cu-Al mixed oxides derived from layered double hydroxides as catalysts for hydrogenation in a flow reactor resulted in the complete hydrogenation of 1,3,5-trinitrobenzene, 2,4,6-trinitrotoluene, 2,4,6-trinitroxylylene, and 2,4,6-trinitromesitylene with a higher selectivity to the corresponding triaminobenzenes that were subsequently hydrolyzed to the phloroglucinol derivatives in good yields (75–82%) [66]. Varying the reaction conditions, the yields of TAB and 2,4,6-triaminotoluene (TAT) double salts with sulfuric acid were increased to 92 and 98%, respectively, while the subsequent hydrolysis of salts resulted in phloroglucinol and methylphloroglucinol in 78

and 91% yields [71]. Supported Cu/SiO₂ catalytic materials seem preferential, especially based on Cu phyllosilicate Cu₂Si₂O₅(OH)₂ (chrysocolla). Even though Cu in ionic forms is considered to be a water pollutant [72], chrysocolla is well known to be a widely spread natural mineral which is stable in the environment [73].

A silica-supported chrysocolla-like phase is widely used as a catalyst precursor. One can find in the article [74] the recent brief review of the methods used for the preparation of the chrysocolla-based materials. The most often used and efficient methods are ammonia evaporation (AE) and deposition–precipitation using urea thermal hydrolysis (DPU), yet several other methods have been used, also. The hydrothermal treatment of the suspension consisting of amorphous silica and Cu(NO₃)₂–NH₃ solution resulted in the formation of the chrysocolla phase with Cu content 32 wt% that was stable after calcination at 350 °C [14]. Its reduction occurred at higher temperatures than its reduction in silica-supported CuO nanoparticles of the size 9.7 nm. After reduction in the calcined sample in an H₂ flow at 250 °C, XRD analysis detected metallic Cu crystallites of an average size of 4.3 nm that is close to the value of 4.1 nm calculated on the basis of the copper surface area, $S_{Cu} = 46 \text{ m}^2\text{g}^{-1}$; however, the Auger spectrum of Cu LMM showed that the ratio $\text{Cu}^+ / (\text{Cu}^+ + \text{Cu}^0)$ was 66%, i.e., reduction was incomplete, in contradiction to the complete reduction in CuO nanoparticles supported on silica. A slow reduction in the precursor for the catalyst 45.5%Cu/SiO₂ (prepared using Aerolyst SiO₂ by the DPU method) in an H₂ flow at 380 °C brings about the formation of the highly dispersed Cu₂O and Cu⁰ phases with CSD (coherently scattering domains) of between 2.5 and 6.5 nm, while after treatment at the reaction conditions (170 °C, 1.3 MPa H₂, 1,4-dioxane as a solvent) of liquid-phase hydrogenation of γ -valerolactone, CSD increased to between 4.0 and 31 nm, respectively [8], indicating recrystallization and sintering in both phases. Surprisingly, the atomic ratio Cu⁰/Cu⁺ strongly decreased, exhibiting Cu⁰ oxidation under reaction conditions. For the initial reduced samples, the measured S_{Cu} value was 15 m²g^{−1}. The reduced (50% H₂/N₂, 250 °C) sample of the preliminarily calcined (500 °C) precursor for the catalyst 16.8%Cu/SiO₂ (prepared using silica gel by the AE method) exhibited far larger S_{Cu} assuming the Cu⁰ particle size of 1 nm, but the TEM average size was 2.2 nm [11]. XPS spectra suggested the presence of Cu⁰, Cu^{δ+}, and Cu²⁺ in the CuSiO₃ phase. Only major reflections of the highly dispersed Cu₂O and Cu⁰ phases were observed in the spent sample after the reaction of methyl formate hydrogenation at 140 °C, 1.3 MPa H₂, the primary crystallite size supposed to be smaller than 2 nm. The XPS spectra of the spent sample are similar to that of a reduced sample. The AE method was also used for the preparation of the catalyst 5%Cu/SiO₂. The sample was calcined at 400 °C and then reduced in a 5%H₂/N₂ flow at 300 °C [13]. The average size of the metallic Cu nanoparticles calculated on the basis of HAADF-STEM images was about 2.9 nm. The XPS and XAES of Cu LMM analysis offered the following relative contents of the Cu species: 20% Cu⁰, 55% Cu⁺, and 25% Cu²⁺. The catalyst was highly stable at reaction conditions of liquid-phase hydrogenation of γ -butyrolactone (170–210 °C, 2–6 MPa H₂; 1,4-dioxane). After five cycles of the reaction (200 °C, 4 MPa H₂), the size of the metallic Cu nanoparticles remained almost unchanged, and the Cu species distribution only slightly shifted to the increase in the Cu²⁺ portion due to oxidation of both Cu⁰ and Cu⁺. The materials prepared by the AE method using SiO₂ with a high surface area (400 m²g^{−1}) exhibited high thermal stability at 0.3–30 wt% Cu, and no CuO was detected using XRD or TEM even after calcination at 600 °C, whereas the XPS data for the sample 10%Cu/SiO₂ showed that the chemical state of copper at the surface was Cu²⁺ [5]. Nevertheless, after the reduction in this calcined sample 10%Cu/SiO₂ in a flow of 10%H₂/He at 300 °C, metallic Cu nanoparticles of the average size 1.5–2.9 nm were found using TEM, and only a slight increase to 2.7–3.6 nm was observed after 500 h on-stream in non-oxidative ethanol dehydrogenation at 280 °C. The XPS results confirmed Cu⁰ formation, and it is the only copper state according to Auger Cu LMM. All of the abovementioned examples demonstrate that the properties of chrysocolla-like precursors and the prepared catalysts strongly depend not only on the preparation procedure and a silicon source, but on the Cu content as well.

Previously [75,76] we have shown that the materials based on the silica-supported chrysocolla-like phase are highly active in the reduction of nitrobenzene and *p*-dinitrobenzene with molecular hydrogen, as well as can be used even for one-pot reduction in trinitrobenzene with a significant yield of amines [74]. In this work, we aimed to reveal the optimal reaction conditions for the catalytic hydrogenation of trinitrobenzene, the first representative of trinitro-aromatic compounds, to triaminobenzene with molecular hydrogen over the catalysts, consisting of a chrysocolla-like phase supported on the commercial low-cost silica carrier, as well as the optimal compositions of these catalysts. It was first shown that even a small decrease in the reaction temperature as compared with that used previously resulted in a significant increase in the reaction time, while lowering an initial H₂ pressure decreased the yields of amines to unacceptably low values. The catalysts with Cu loading varying in a wide range of 3–15 wt% were prepared for the first time on the commercial meso-macroporous silica carrier with a low surface area and were tested in TNB reduction with hydrogen. It was revealed for the first time that complete TNB conversion with a 50–65% selectivity to TAB can be reached for the catalysts with a Cu loading of 8–15 wt%, and calcination at 600 °C enhanced the activity, selectivity, and stability of these catalysts.

2. Results

2.1. Effect of Reaction Temperature, Initial Hydrogen Pressure, and Reaction Time

The effect of reaction conditions on the catalyst's behavior has been studied using the example of a catalyst with an average Cu loading of 8% calcined at 300 °C. At the initial hydrogen pressure of 1.3 MPa, the TNB conversion started at 150 °C in 1 h and was completed in 5 h (Figure 1a), the major amines being 3,5-dinitroaniline (DNA) and 5-nitrophenylene-1,3-diamine (NPDA). Hydrogenation of nitro groups proceeded consequently. Further hydrogenation at these conditions resulted in an almost complete nitro group reduction to an amino group with a TAB yield of 67%. The slight increase in the reaction temperature from 150 to 170 °C drastically enhanced the catalytic activity, but decreased the selectivity to amines (Figure 1b). TNB disappeared in the reaction solution in 1 h already, the overall selectivity to amines (DNA and NPDA) being only 40%. The only amine product after 2 h of the reaction was TAB with a yield of 50%.

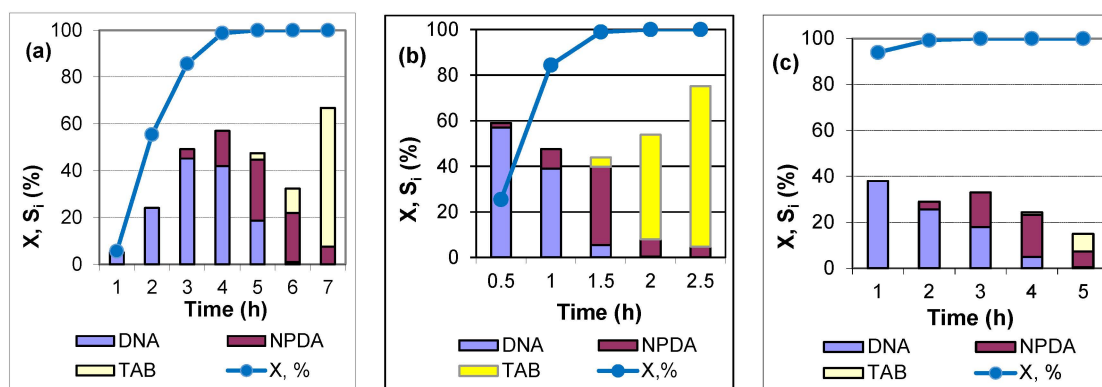


Figure 1. Dependence of the TNB conversion (X) and selectivity to individual amines (S_i) versus the reaction time for the sample 8Cu-300 at different reaction conditions: (a) $T = 150$ °C, $P = 1.3$ MPa; (b) $T = 170$ °C, $P = 1.3$ MPa; (c) $T = 170$ °C, $P = 0.5$ MPa.

The decreased yield of aromatic amines may be due to both the enhanced TNB chemisorption on the free silica surface and formation of intermediates that cannot be detected with GLC. The test with the silica support at these conditions revealed a considerable decrease in the TNB concentration (30% in 1 h, 40% in 3 h), whereas no amine was detected. The decrease in the initial hydrogen pressure to 0.5 MPa at 170 °C resulted in considerably lower catalytic activity, and the overall selectivity to amines was the lowest (Figure 1c). Therefore, the reaction temperature 170 °C and initial hydrogen pressure 1.3 MPa were selected for further studies.

2.2. Effect of Thermal Treatment

The catalytic activity of the dried catalysts with Cu loading 3–6% was low, and only DNA was observed with a low selectivity. The prepared catalysts with a higher Cu loading of 9–10% exhibited catalytic activity with the formation of expected amines even after drying (Figure 2a), yet calcination at 300 °C strongly enhanced their activity (Figure 2b). Complete TNB conversion with a high yield of amines has been achieved in 1–1.5 h, the intermediate compounds being the major products. The complete reduction to TAB required a longer reaction time. For example, the TNB hydrogenation to TAB with a selectivity of 52% has been reached in 2 h over the calcined catalyst 11Cu-300, whereas the TNB conversion was complete in 1 h (Figure 2b). Calcination at 600 °C, which can bring about the chrysocolla dehydration to a large extent, results in the material with the highest activity and selectivity to TAB (Figure 2c). The selectivity to TAB was 82% at the complete TNB conversion in 1 h.

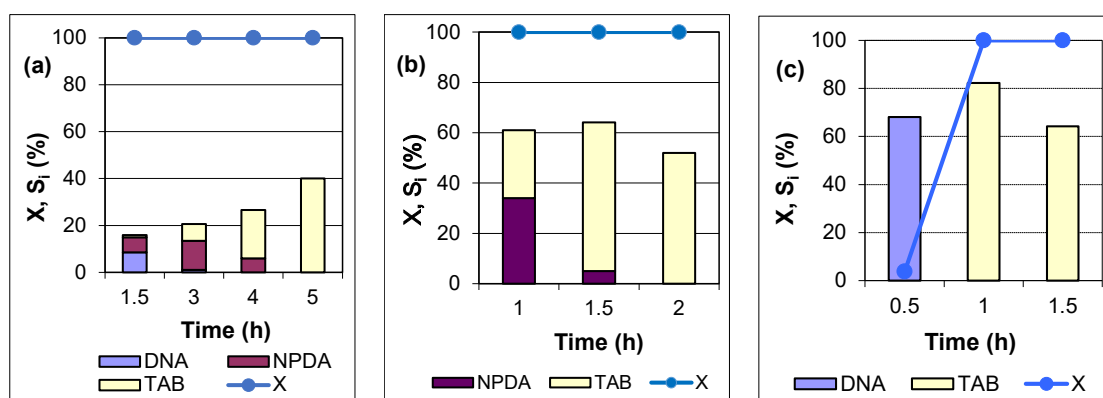


Figure 2. Dependence of the TNB conversion (X) and selectivity to individual amines (S_i) versus the reaction time for the sample 10Cu-T after different thermal treatments: (a) drying at 110 °C; (b) calcination at 300 °C; (c) calcination at 600 °C. Reaction conditions: $T = 170$ °C, $P = 1.3$ MPa.

The following explanation for the effect of calcination can be proposed based on the results obtained in this work and on the analysis of publications that concerned chrysocolla-like phyllosilicate synthesis, structure, and properties. There are two requirements for hydrogenation with molecular hydrogen to proceed: (i) dissociative adsorption of molecular hydrogen, and (ii) activating the adsorption of a substrate. In Cu phyllosilicate catalysts, the adsorption and dissociation of molecular hydrogen was claimed to occur on the SiO_2 surface [43] or at the $\text{Cu}^{n+}\text{-O-SiO}_x$ interface [9,43]. Chrysocolla is stable to reduction by molecular hydrogen up to 180–215 °C [9,77,78]. For this reason, the Cu catalysts are commonly activated by pre-reduction in hydrogen in order to bring about the complete or partial destruction of the octahedral first coordination oxygen environment of Cu^{2+} ions, resulting in Cu^+ and Cu^0 [8–14]. In the present work, both dried and calcined samples were not subjected to the reduction prior to the catalyst testing. Moreover, the reaction temperature of 170 °C was considerably lower than the temperature of reduction for the dried sample that occurred predominantly at 250–350 °C [74–76]. Therefore, the considerable amount of Cu^{n+} is available in the dried material at the beginning of the reaction and may form the sites for hydrogen dissociation. On the other hand, for the dried samples, TNB adsorption on the coordinatively saturated Cu^{2+} species of the phyllosilicate phase may occur only via substitution of H_2O molecules with the nitro group of TNB, and such process proceeds slowly. In addition, in the presence of the SiO_2 carrier, we revealed a significant decrease in the TNB concentration in the reaction solution at the reaction conditions (30% in 1 h, 40% in 3 h), which indicates TNB adsorption on the SiO_2 carrier surface, which may be irreversible or even followed by formation of other products. Both processes can contribute to the low selectivity of the formation of the considered amines, while the formation of other intermediates cannot be excluded. After calcination at 300 °C,

the structural water has been deleted, opening sites for TNB adsorption, and the new catalytically active Cu^{2+} sites appear in the phyllosilicate structure due to the removal of OH groups that partially damage the phyllosilicate structure, especially at $600\text{ }^{\circ}\text{C}$ [9]. It was shown [5,79] that a band at 670 cm^{-1} , which is distinctive of Cu phyllosilicate [80], can still be observed in FTIR spectra for the samples calcined at $400\text{ }^{\circ}\text{C}$, whereas it was no longer observable after heating to $600\text{ }^{\circ}\text{C}$, and the resulting phase was X-ray amorphous in a sample with a Cu loading of 10%.

2.3. Effect of Cu Loading in the Catalysts

The catalytic activity enhanced strongly with increasing Cu loading in a catalyst (Figure 3). The sample 3Cu-300 exhibited a higher TNB consumption than the support, and in 4–5 h, no TNB was observed. However, only the first reduction product, DNA, was detected in the reaction mixture with a selectivity as low as 20%, which did not change after increasing the reaction time (Figure 3a). Almost complete TNB conversion for the reaction time 5 h was found over the sample 6Cu-300, with the selectivity to DNA increasing with time. Its maximum was triple that of 3Cu-300, and even NPDA and TAB were detected in a reaction mixture in a significant amount (Figure 3b).

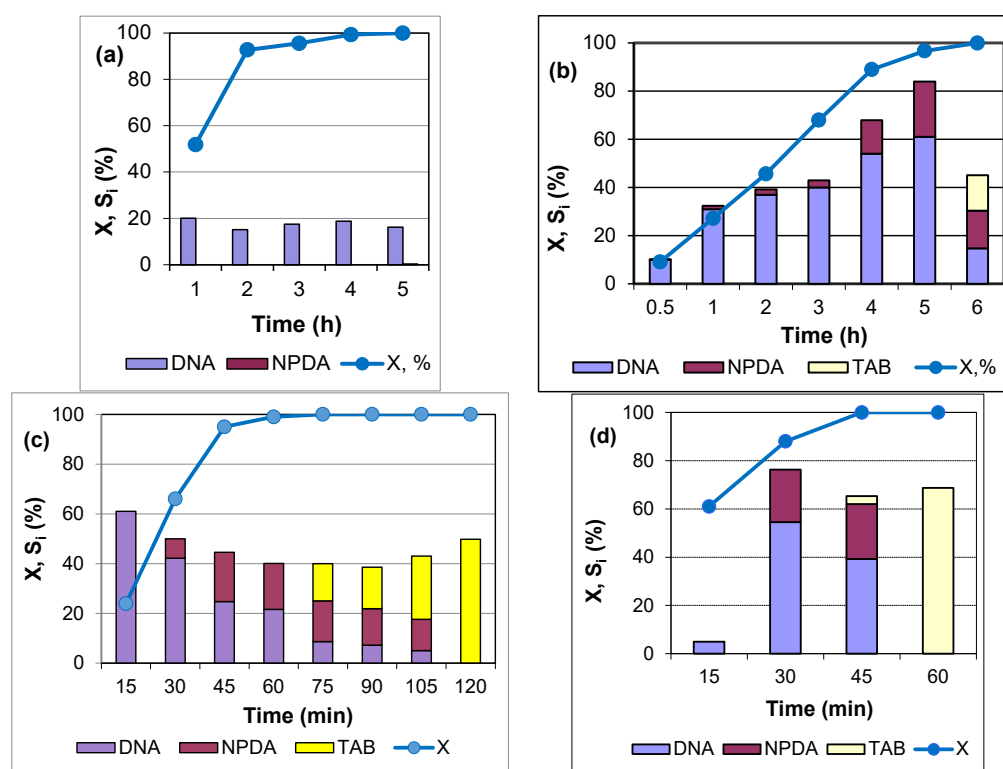


Figure 3. Dependence of the TNB conversion (X) and selectivity to individual amines (S_i) versus the reaction time for the samples calcined at $300\text{ }^{\circ}\text{C}$ with a different Cu loading: (a) 3%; (b) 6%; (c) 9%; (d) 15%. Reaction conditions: $T = 170\text{ }^{\circ}\text{C}$, $P = 1.3\text{ MPa}$.

The overall selectivity to DNA+NPDA reached a highest value of 84%, and then it dropped with the TAB appearance at the complete TNB conversion, thus indicating the formation of a large amount of undetectable intermediates or condensed products (di- and trimers of TAB molecules [81]), during or after hydrogenation of the third nitro group. Similar behavior was observed for the samples with the higher Cu loading of 9–15% (Figure 3c,d).

Further hydrogenation of the last nitro group proceeds over these samples, and the selectivity to TAB rises up to 50–70% with the time shortened to 1–2 h. The larger the Cu loading, the less time required for complete TNB conversion and hydrogenation of all nitro groups to amino groups. The highest activity was obtained for the sample with Cu loading 15%.

The observed moderately low selectivity to aromatic amines may be due to both the fast enhanced TNB chemisorption on the free silica surface and the formation of intermediates that cannot be detected with GLC. The test with the silica support at these conditions revealed a considerable decrease in the TNB concentration (30% in 1 h, 40% in 3 h), whereas no amine was detected. The decrease in the TAB yield with time at the chosen reaction conditions may be caused by its condensation, which was confirmed on the catalysts of a different nature, including Cu catalysts [64,71,81].

2.4. Stability

The most active catalysts were tested for the possibility of further use in hydrogenation of a new portion of the reaction mixture (recycling), and the results are presented in Table 1. Between test cycles, the sample of the material was only separated from a mixture of reaction products by centrifuging, without any intermediate treatment. The activity of the 10Cu-300 material decreased considerably after the first test as compared with the initial sample, which is cleared from a more prolonged time of complete TNB conversion in the second cycle and too low selectivity to TAB even in 7 h. Therefore, this material can be used only for one batch reduction. The material with the larger Cu loading 15Cu-300 is more stable, despite the fact that the catalytic activity of fresh materials is similar. Although the time of complete TNB conversion and reduction to TAB over the used 15Cu-300 samples increased, the selectivity to TAB remained relatively high in two batches. The more profitable usage in two cycles with a gradually higher selectivity to TAB is possible for the 10Cu-600 catalyst calcined at 600 °C; therefore, this catalyst can be recommended for practical application.

Table 1. Results of recycling tests.

Catalyst	Cycle	Reaction Time ^a , h	Selectivity to TAB, %
10Cu-300	1st	2	52
	2nd	7	21
15Cu-300	1st	1.5	65.4
	2nd	4	50.8
	3rd	6	45.7
10Cu-600	1st	1	82.3
	2nd	2	88.1
	3rd	6	45.2

^a Reaction time required for complete TNB conversion.

Withdrawal of TAB from a reaction mixture, for example, via the formation of insoluble salts, seems promising to enhance the selectivity to TAB and stability [65,70]. However, in the recent works of different research groups, deactivation of catalysts under conditions of TNB hydrogenation was observed for both the 1%Pd/C catalyst [64] and the mixed layered CuAlO_x catalyst [71], even though TAB was quantitatively isolated from the reaction mixture in the form of the double salts with sulfuric acid. Two possible mechanisms of the catalyst deactivation were proposed [71]: (i) the formation of high-molecular-weight resinous by-products on the catalyst's surface via polycondensation of TAB molecules, which was shown also by other authors [81], or (ii) the formation of azoxy, azo, and hydrazo compounds via condensation of nitrosoarenes and arylhydroxylamines (common intermediate products of the nitroarene reduction [18,63,66,82]). In view of the fact that the concentrations of resinous substances on the catalyst surfaces at the reactor inlet were higher than those in the middle part and at the outlet, the second mechanism seems to prevail. These deposits can be removed by sample calcination in air at 330 °C.

2.5. Characterization of the Catalysts

In order to clarify the possible reasons of the revealed catalytic behavior of the catalysts prepared, their phase composition, morphology, texture, and reducibility were characterized. All of the prepared catalysts were subjected to an XRD phase analysis, and the obtained results

confirmed the presence of two predominant phases, i.e., silica in all samples and the chrysocolla-like phase if Cu loading was within 10–15% (Figure 4 and Figure S1). The SEM-EDX analysis showed a uniform distribution of Cu in the catalysts prepared (Figure 5).

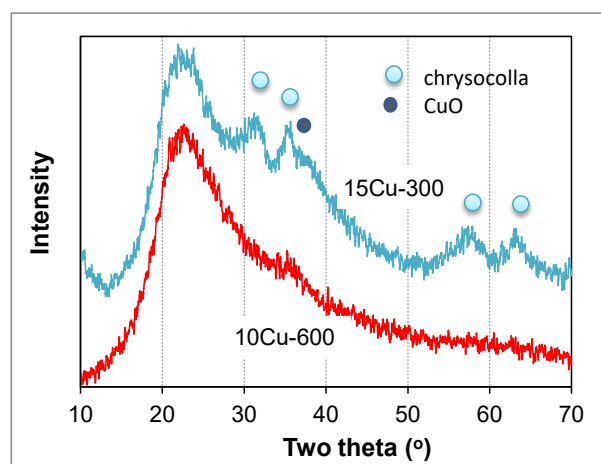


Figure 4. XRD patterns of the catalysts 15Cu-300 calcined at 300 °C, and 10Cu-600 calcined at 600 °C.

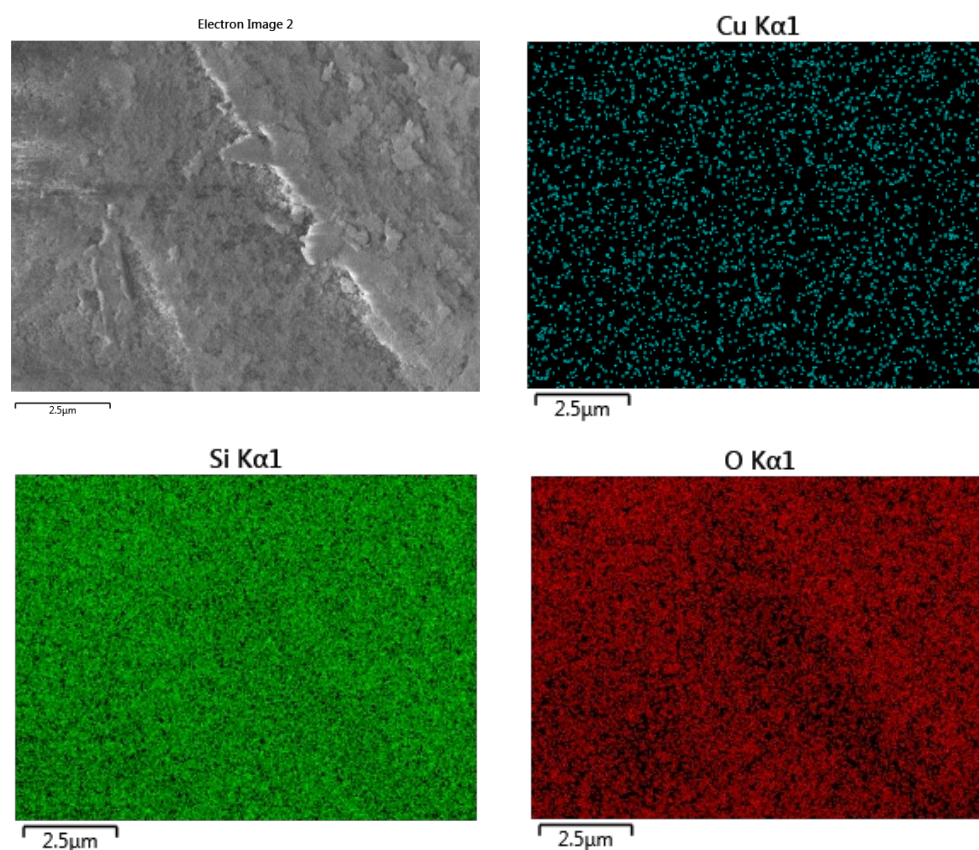


Figure 5. SEM image at low magnification and SEM-EDX maps of element distribution for the catalyst 10Cu-110.

The morphology of the materials prepared was studied, and the typical selected SEM and TEM images are depicted in Figures 6 and 7. The SEM images at high magnification for both the materials dried and calcined at 300 °C only (Figures 6a and 7a) exhibited a uniform porous solid consisting of aggregated particles of less than 100 nm in size. In addition to these nanoparticles, lamellar structure sheets and their loose aggregates were present in the samples. Moreover, in the SEM images for the samples calcined at 300 °C, the foam-like

micron-sized arrays are observed (Figure 7a). The TEM images exhibit that the arrays consist of extended needle-like shapes, and the isolated dark round spots of a size less than 4 nm are visible on their surface (Figure 7b). TEM images exhibit numerous isolated dark spots and clearly recognized crystallites of 4–25 nm in size on the surface of the SiO₂ particles (Figure 6b,c and Figure 7c,d) that are presupposed to be the chrysocolla-like nanoparticles.

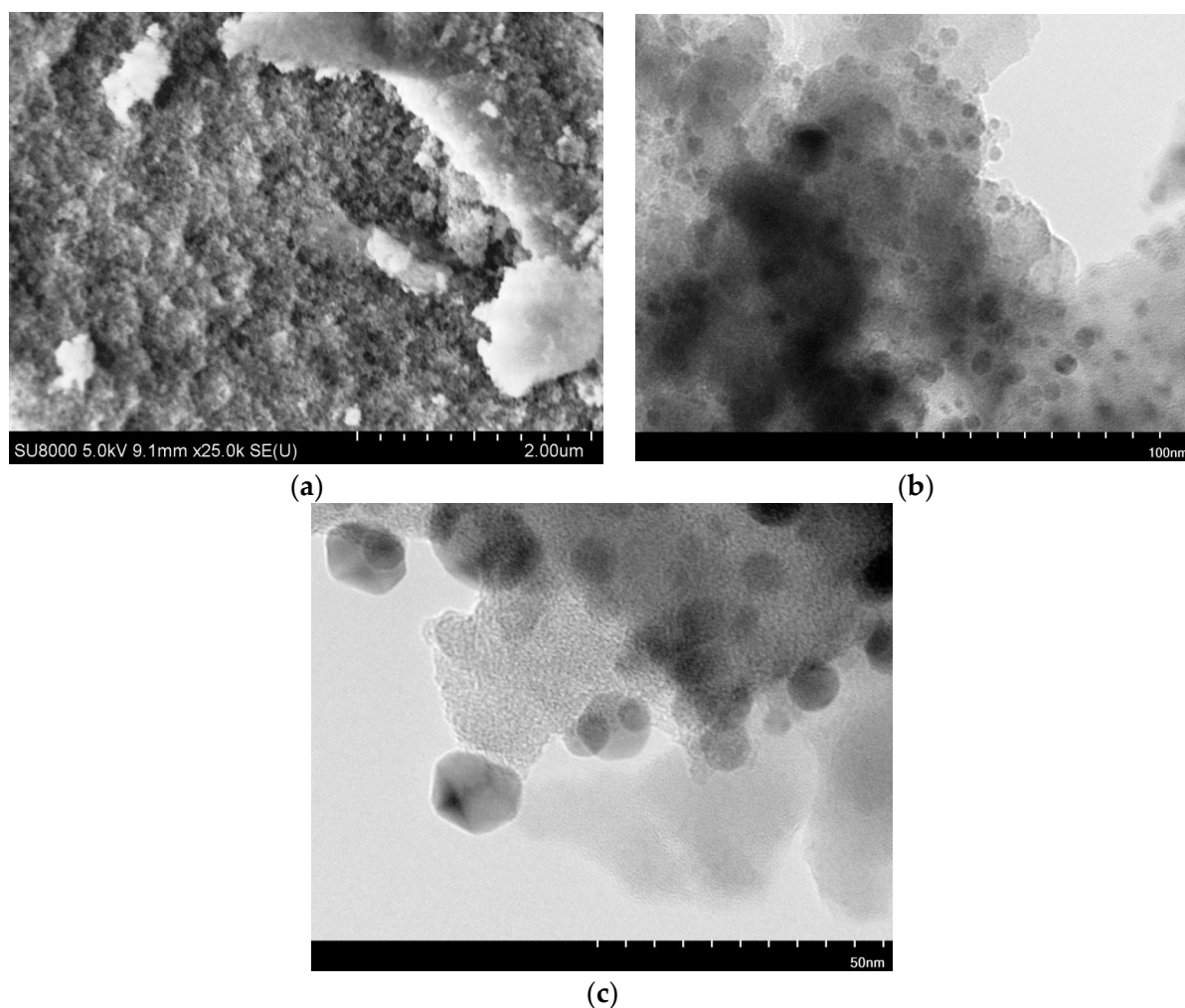


Figure 6. SEM image at high magnification (a) and TEM images (b,c) of the sample 10Cu-110.

According to the IUPAC classification, N₂ adsorption–desorption isotherms exhibited by the synthesized catalysts (Figure S2) can be characterized as the type IV isotherms with a superposition of H1, H3, and H4 hysteresis loops that suggested the presence of a narrow distribution of the ink-bottle-shaped pores and the slit-like pores in non-rigid aggregates of plate-like particles [83,84]. The observed pronounced N₂ uptake at low p/p° (Figure S3) can be associated with the filling of micropores [83,84]. The values of the specific surface area S_{BET} and meso- and micropore volume are listed in Table 2, as well as the pore size distributions, which are illustrated in Figure 8a–d. The specific surface area increased drastically with increasing Cu loading in the range of 6–15%, whereas calcination at 300 °C did not affect its value. The increase in S_{BET} can be due to the formation of a chrysocolla-like phase that is featured with the extremely high specific surface area values of about 700 m²g^{−1} [78,80]. After calcination at 600 °C, S_{BET} decreased slightly due to the disappearance of micropores (sample 10Cu-600). Both the volume of pores of the size below 300 nm and the mesopore volume decreased significantly with increasing Cu loading in the range

of 10–15%, while the micropore volume increase was confirmed by calculations vs. the DFT-cylinder model method and by Sing's α_s -method [85].

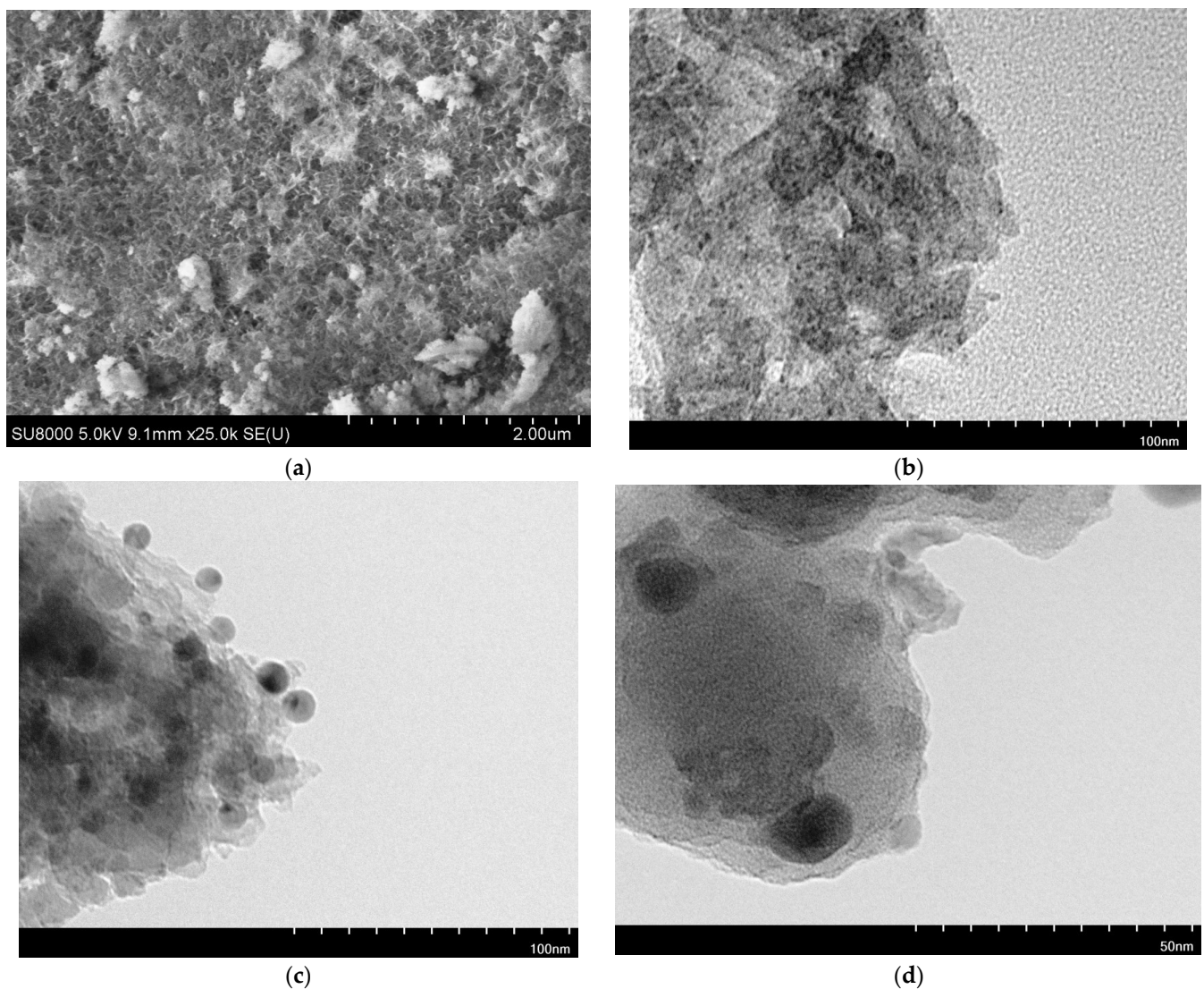


Figure 7. SEM image at high magnification (a) and TEM images (b–d) of the sample 10Cu-300.

Table 2. Textural features of the initial silica support and the catalysts prepared.

Sample	S_{BET} , m^2g^{-1}	$V_{\text{total}}^{\text{a}}$, cm^3g^{-1}	$V_{\text{meso}}^{\text{b}}$, cm^3g^{-1}	V_{micro} (DFT-Cylinder), cm^3g^{-1}	$V_{\text{micro}}(\alpha_s)$, cm^3g^{-1}
SiO ₂	100	0.671	0.661	0.010	0.004
6Cu-300	213	0.661	0.652	0.009	0.009
10Cu-110	251	0.615	0.593	0.017	0.021
10Cu-300	250	0.639	0.625	0.014	0.015
10Cu-600	224	0.589	0.589	0	0
15Cu-300	319	0.603	0.582	0.021	0.018

^a Adsorption at $p/p^0 = 0.99$. ^b $V_{\text{meso}} = V_{\text{total}} - V_{\text{micro DFT}}$.

The mesopore size distributions in the prepared catalysts strongly differ from that of the initial support, i.e., the monomodal narrow distribution with a maximum at 23 nm in the SiO₂ carrier is transformed into the wide bimodal distribution with two definite maxima at 3 nm and 12–19 nm (Figure 8a,b). Neither Cu loading nor calcination temperature affected the position of the former one, whereas the position of the latter one shifted to smaller

sizes with the increase in Cu loading, as well as after calcination at 600 °C. In addition, the volume of mesopores of the size 2–5 nm increased with increasing Cu loading. Similar changes in the silica mesopore distributions were observed previously and were attributed to the silica dissolving under urea hydrolysis at 90 °C followed by deposition–precipitation of the chrysocolla-like phase [86].

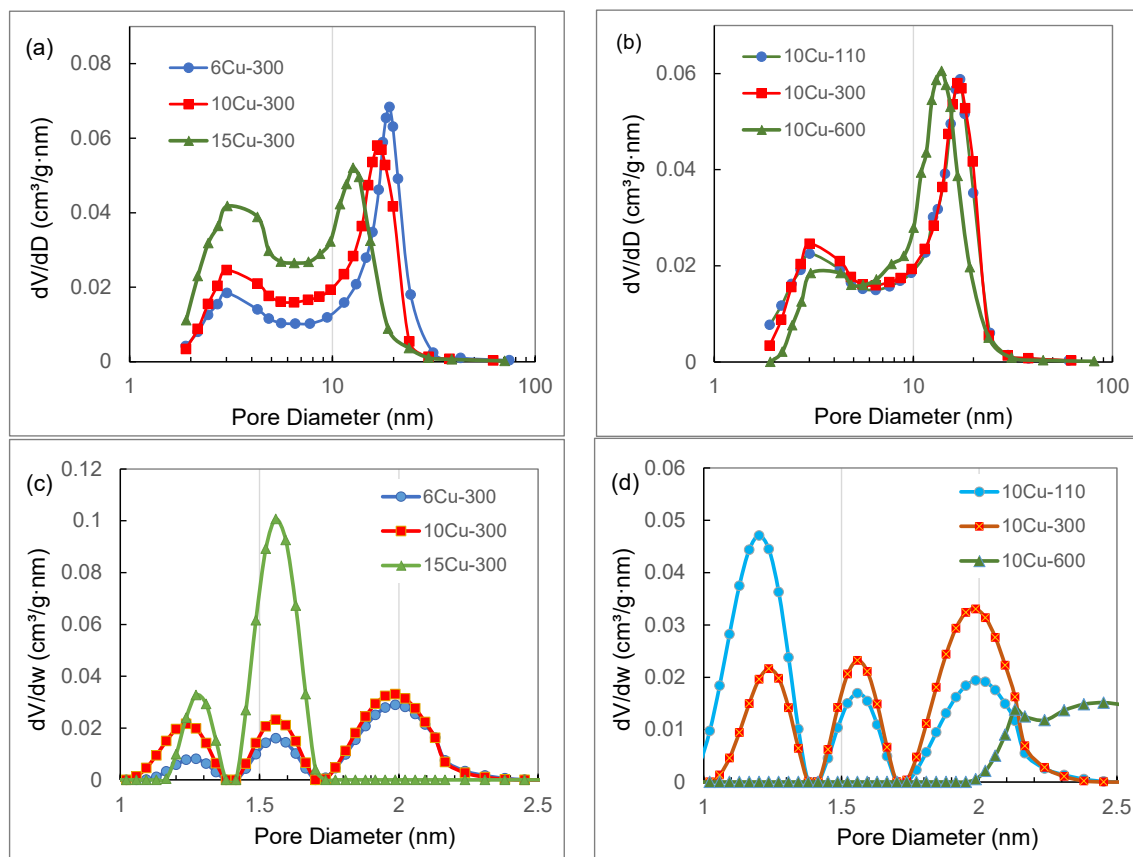


Figure 8. The mesopore size distribution curves (a,b) and the micropore size distribution curves (c,d) for the $\text{Cu}_2\text{Si}_2\text{O}_5(\text{OH})_2/\text{SiO}_2$ catalysts differed in Cu loading (a,c) and in the temperature of thermal treatment (b,d).

The DFT-cylinder model gives the trimodal micropore size distributions for the prepared $\text{Cu}_2\text{Si}_2\text{O}_5(\text{OH})_2/\text{SiO}_2$ catalysts (Figure 8c,d) with maxima at 1.2, 1.6 nm, and 2.0 nm. The volume of thin micropores increased with increasing Cu loading, yet decreased with increasing temperature of final treatment, which made possible to attribute them to the chrysocolla-like phase. Hence, the synthesized chrysocolla-like $\text{Cu}_2\text{Si}_2\text{O}_5(\text{OH})_2/\text{SiO}_2$ catalysts possess a high specific surface area and a micro-mesoporous texture with a bimodal mesopore size distribution, which is due to the formation of the highly dispersed microporous chrysocolla phase.

The TPR- H_2 profiles of the $\text{Cu}_2\text{Si}_2\text{O}_5(\text{OH})_2/\text{SiO}_2$ catalysts, as well as the total hydrogen consumption (as $\text{H}_2:\text{Cu}$ molar ratio), are presented in Figure 9. Figure 9a also displays the TPR- H_2 profiles of the reference CuO/SiO_2 sample prepared using the deposition–precipitation procedure using urea thermal hydrolysis (DP). The TPR profile of this reference sample shows a single broad peak in the range 130–350 °C (the major part in the range 170–300 °C) centered at 260 °C, and the calculated value of hydrogen consumption is close to the stoichiometric one calculated for the complete reduction of CuO to metallic Cu . Reduction of the dried chrysocolla-like catalysts, 10Cu-110 and 3Cu-110, proceeded at considerably higher temperatures from 200 °C up to 350 °C (temperatures of the major range increased with a Cu loading decrease), with the reduction peak maximum centered between 295 and 315 °C, respectively (Figure 9a). It should be pointed out that the calculated value

of hydrogen consumption is half as much against the stoichiometric one for both samples. The almost symmetric broad reduction peaks for the calcined chrysocolla-like catalysts are shifted to lower temperatures of 150–280 °C, the maximum centered at about 250–255 °C, being independent of Cu loading (Figure 9b). A similar decrease in the reduction temperature for calcined at 430 °C samples as compared with a dried one was observed earlier [78], and it was attributed to formation of the highly dispersed silica-supported CuO particles due to the thermal dehydration of Cu hydrosilicate under calcination. Our TEM observation of the appearance of nanoparticles smaller than 4 nm (Figure 7b) and very weak XRD reflection of the CuO phase in the XRD pattern of the sample 15Cu-300 (Figure 4) is the evidence in favor of this assumption. Moreover, the values of hydrogen consumption for the calcined samples decreased (Figure 9b). The values of hydrogen consumption by chrysocolla-containing catalysts, both dried and calcined, exceed the values required for reduction of Cu^{2+} to Cu^0 . We proposed [74] that increased hydrogen consumption could be due to formation of the surface Si–O–H groups instead of the bridge bonds Si–O–Cu destructed during a complete reduction in chrysocolla with hydrogen. Previously [78], formation of additional silanol groups was revealed as the increase in the intensity of the band at 3740 cm^{-1} in the DRIFT spectra during reduction in chrysocolla-like phases in pure hydrogen. Therefore, the ratio $\text{H}_2:\text{Cu} > 1$ may be attributed to the reduction of the chrysocolla-like structure. It should be mentioned that for the similar sample calcined at 600 °C, the value of the ratio $\text{H}_2:\text{Cu}$ was in agreement with the one calculated for the complete reduction of CuO to metallic Cu, and it has been ascribed to a reduction in X-ray amorphous CuO nanoparticles [5]. The TPR analysis revealed considerable distinctions in the reducibility of the $\text{Cu}_2\text{Si}_2\text{O}_5(\text{OH})_2/\text{SiO}_2$ and CuO/SiO_2 samples, as well as its variations depending on the Cu loading and calcination temperature of the $\text{Cu}_2\text{Si}_2\text{O}_5(\text{OH})_2/\text{SiO}_2$ catalysts, which could be one of the reasons for the different catalytic behavior in the hydrogenation process. A partial reduction to metallic Cu seems to be possible at the reaction conditions used in the present work. The metallic Cu^0 nanoparticles and Cu^+ species were observed previously in the similar catalysts used at the similar hydrogen pressures and temperatures for one-pot hydroamination of 5-HMF with nitro-compounds [76]. On the other hand, we also revealed that the fast selective reduction of both nitrobenzene and *p*-dinitrobenzene to amines with molecular hydrogen occurred on the silica-supported Cu catalysts that were not subjected to preliminary reduction [76].

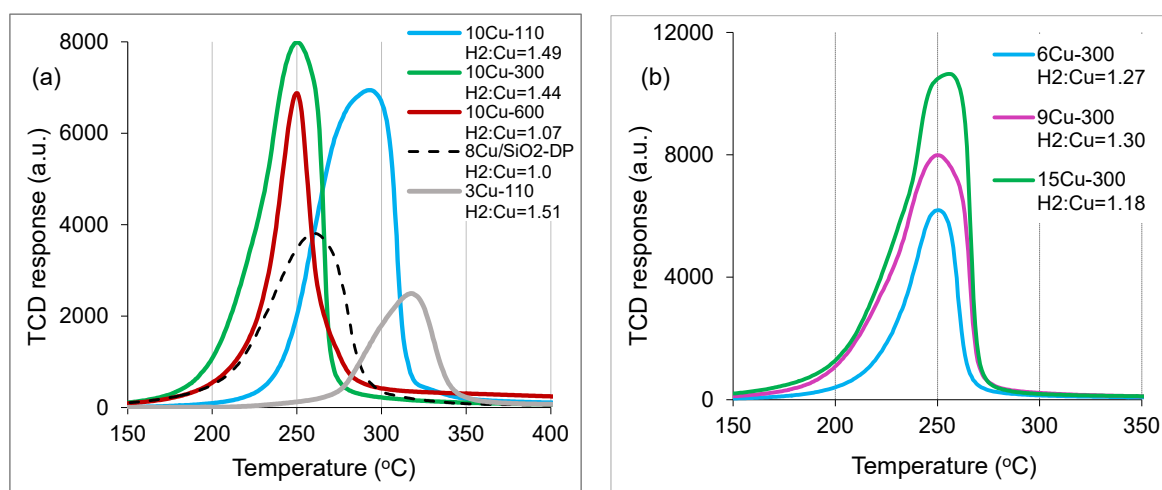


Figure 9. TPR profiles of the $\text{Cu}_2\text{Si}_2\text{O}_5(\text{OH})_2/\text{SiO}_2$ catalysts dried and calcined at different temperatures (a) and differed in Cu loading (b), as well as CuO supported on silica by the deposition-precipitation procedure using urea thermal hydrolysis (8Cu/SiO₂-DP).

When the results of the physico-chemical characterization of materials are compared with the data on their catalytic behavior in the selective hydrogenation of TNB to amines, it

is apparent that the following scheme of the catalytic process may be proposed depending on the catalyst's composition (Figure 10).

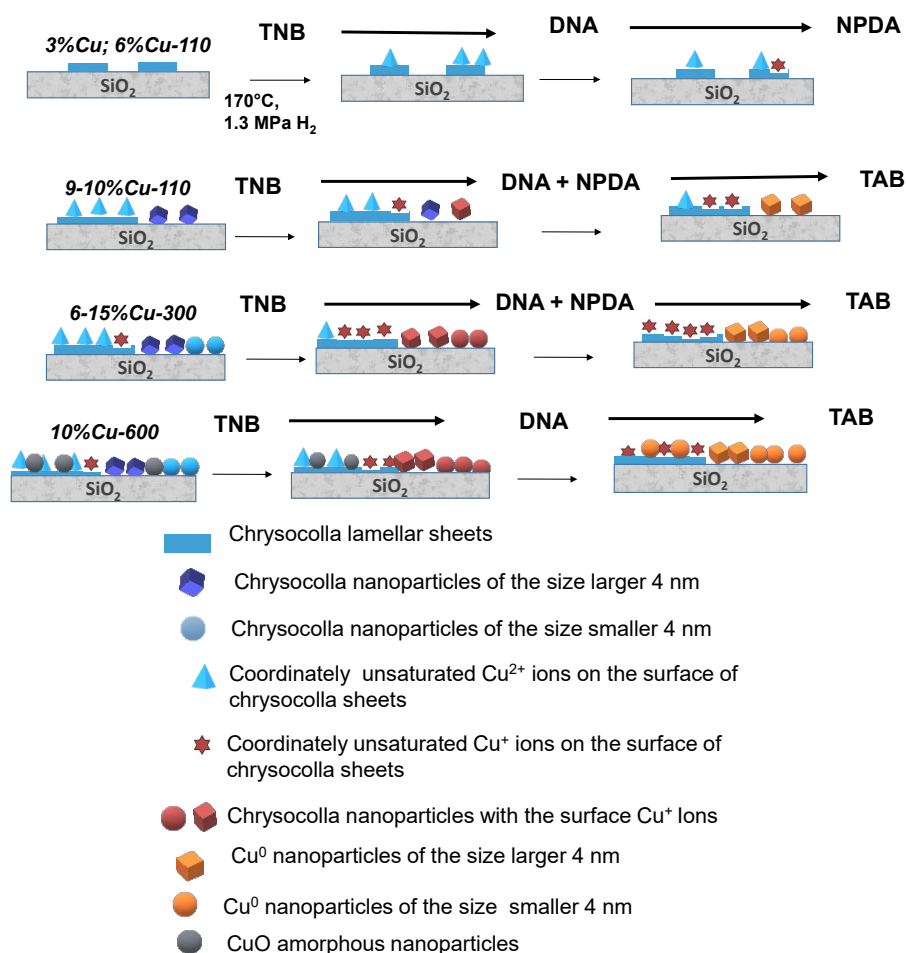


Figure 10. Scheme of possible catalyst transformations under reaction conditions and the associated catalytic formation of amines.

The small isolated lamellar chrysocolla-like surface species ($\text{Cu}_2\text{Si}_2\text{O}_5(\text{OH})_2 \cdot x\text{H}_2\text{O}$) arising in the course of the synthesis of the sample with a low Cu loading are highly stable to reduction with hydrogen (Figure 9a) and show low activity in TNB hydrogenation to amines (Figure S4a). They exhibited the significant catalytic activity in TNB hydrogenation only after calcination at 300 °C (Figure 3a,b and Figure S4b) when the appearance of coordinately unsaturated Cu²⁺ ions became possible due to partial dehydration and dehydroxylation of the chrysocolla surface [74,77–80]. The sample 3Cu-300 catalyzed the slow reduction in only one nitro group with a low selectivity (Figure 3a), which may be due to the parallel occurrence of other TNB transformations [62–67,70,71,81] both on the chrysocolla and silica surface. Prolonged treatment with H₂ at reaction conditions (170 °C, 1,3 MPa) may result in the slight reduction in the catalyst's surface with formation of the Cu⁺ sites for further DNA reduction to NPDA (Table S1, catalyst 3Cu-300). When Cu loading is doubled (sample 6Cu-300), the number and the surface of chrysocolla nanoparticles can be increased, enhancing DNA formation due to inhibiting TNB adsorption and side reactions on the active silica surface via interaction with Cu²⁺ or (and) covering with the chrysocolla species. In consequence of this, the TNB conversion decreases, whereas the selectivity of slow hydrogenation of nitro groups considerably increases (Figure 3b). Moreover, due to easier material reducibility (Figure 9b), the surface Cu⁺ and Cu⁰ active sites for hydrogenation of the second and third nitro groups can appear at the reaction conditions. The reflections of metallic copper were observed in the XRD pattern of the catalyst, similar

to 12Cu-300 used in hydroamination of 5-HMF with aromatic nitro compounds at reaction conditions that are fairly analogous to those applied in the present work (150–170 °C, initial hydrogen pressure of 1.0 MPa, THF as a solvent) [87]. Both Cu⁰ and Cu⁺ surface species were revealed in this catalyst by the deconvolution of the Cu2p_{3/2} Auger peak in the Cu LMM XAES spectrum [87]. The further increase in Cu loading can give rise to a larger number of the chrysocolla nanoparticles and enhance their reducibility in the range of 170–200 °C (Figure 9b), which results in the higher TNB conversion and selectivity to TAB in considerably shortened reaction times (Figure 3c,d). It should be figured out that the initial calcined catalytic materials with a high Cu loading can already contain copper in the electronic state Cu⁺. Deconvolution of the Cu2p_{3/2} XPS spectrum of the catalyst similar to 12Cu-300 revealed a low intensity peak at 932.2 eV attributed to Cu⁺ [87]. The relative concentration of Cu⁺ was estimated to be 8%.

Calcination of the materials at 600 °C may result in the almost complete decomposition of the chrysocolla phase to X-ray amorphous CuO and SiO₂, as was observed previously [75]. No diffraction peaks of Cu-related phases were observed after calcination at 600 °C, while the bands due to Cu phyllosilicate in FTIR spectra were still observable, with the exception of the δ_{OH} band. By this means, the numerous coordinatively unsaturated Cu²⁺ sites arise on the phyllosilicate surface, forming grain boundaries with highly dispersed CuO species. Such structures seem to possess extremely high catalytic activity in hydrogenation of nitro groups in TNB.

The following possible scheme of TNB hydrogenation to aromatic amines can be proposed (Figure 11):

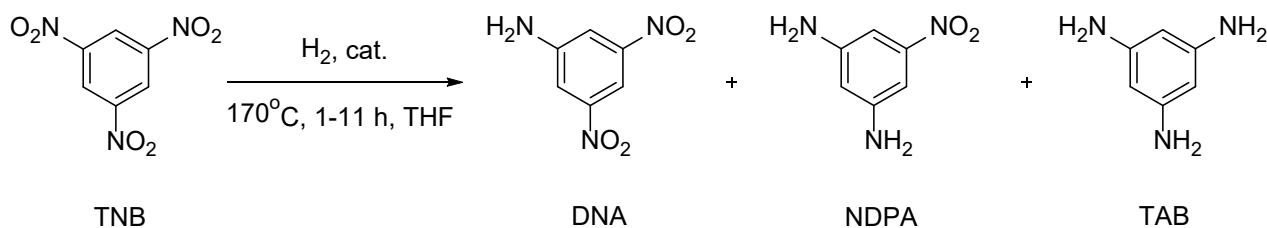


Figure 11. Simplified scheme of 1,3,5-trinitrobenzene hydrogenation to amines.

3. Materials and Methods

3.1. Materials and Synthesis

Silica-supported chrysocolla-like Cu₂Si₂O₅(OH)₂/SiO₂ materials were prepared by the method of deposition–precipitation using urea (DPU) in accordance with the previously described procedure [74]. The commercial meso-macroporous silica carrier (S_{BET} = 98 m²g^{−1}; V_{pore} = 1.05 cm³g^{−1}) (KhimMed, Moscow, Russia), urea (Acros Organics, Geel, Belgium), and Cu(NO₃)₂·3H₂O (Aldrich) were used for synthesis. A suspension of silica in an aqueous solution of the required mass of urea and Cu(NO₃)₂ was heated to 92 °C and kept at this temperature for 8 h. The resulting solid was separated by centrifuging at room temperature, washed with distilled water, and was consequently dried in a rotor evaporator and in an oven. Thermal treatment of dried samples were consequently performed at 110 °C, 300 °C, and 600 °C for 4 h. Cu loading in the samples was varied from 3 wt% to 15 wt%, and the upper loading limit is due to the formation of a CuO phase during the material calcination at 300 °C. The synthesized materials were designated as ACu–T, where A is a Cu loading and T is the temperature of the final thermal treatment, °C.

3.2. Characterization of Materials

The XRD analysis was performed using an ARL X'TRA (Thermo Fisher Scientific, Waltham, MA, USA) diffractometer equipped with a theta–theta goniometer (CuKα radiation, 2θ = 5°–70°, a scanning rate 1° min^{−1}, CCDC data files). FE-SEM Hitachi SU8000 (Tokyo, Japan) field-emission scanning electron microscope and TEM Hitachi transmission electron

microscope was used to observe the sample morphology, and images were acquired at the 100 kV accelerating voltage in the bright-field TEM mode. EDX studies were carried out using an Oxford Instruments X-max EDX system (Abingdon, UK). The N₂ adsorption–desorption isotherms were obtained using an ASAP 2020 Plus unit (Micromeritics, Norcross, GA, USA). To determine the textural characteristics, we performed an isotherm analysis followed the BJH and DFT methods [74]. Reducibility of the samples was studied by temperature-programmed reduction with hydrogen (TPR-H₂); the conditions were as follows: 5% H₂/Ar (30 mL min⁻¹), heating ramp 10 °C min⁻¹ up to 500 °C.

3.3. Catalytic Activity Test

The samples were tested in the selective TNB hydrogenation in batch mode. A 100 mL laboratory autoclave with Teflon insertion was poured with reaction mixture (tetrahydrofuran (THF)—15 mL, TNB—0.200 g, 0.100 g of eicosane (internal standard for GLC)—0.100 g, a catalyst—0.100 g, pure H₂ (the initial pressure 0.5–1.3 MPa), and then heated to the reaction temperature of 150–170 °C. Mass ratio TNB:catalyst was 2:1, while molar ratio TNB:Cu varied from 4.1 to 20.7 depending on Cu loading. In the experiments on the stability of the catalytic properties, the reaction conditions differed slightly: 30 mL of THF, 0.400 g of TNB, 0.200 g of catalysts. Intermediate washing of a sample and an autoclave system with THF for 1 h was used between cycles. The GLC analysis of the liquid probes, which were withheld from the reactor several times during the reaction process, was performed using a CrystaLux 4000M GLC instrument (a 30 m × 0.25 mm capillary S2 column Optima-1, Macherey-Nagel, Düren, Germany) in the temperature-programmed mode (initial heating to 150 °C, keeping at this temperature for 6 min, heating from 150 to 240 °C at the rate of 20 °C min⁻¹, and keeping at 240 °C for 10 min). In addition to 1,3,5-triaminobenzene (TAB), two other amine intermediates were revealed: 3,5-dinitroaniline (DNA), and 5-nitrophenylene-1,3-diamine (NPDA) (Figure 11). The changes in the relative concentrations in the reaction system TNB–DNA–NPDA–TAB with time, which were corrected to the area of a standard peak in an initial reaction mixture, were used to calculate the TNB conversion and the selectivity to the individual amines.

It should be mentioned that the reduction of trinitroarenes with molecular H₂ is a complicated process resulting in the formation of intermediates and products that cannot be detected using GLC [62–67], yet we considered only amines that can be considered to be useful chemicals.

4. Conclusions

The catalysts with a Cu loading of 3–15 wt% consisting of chrysocolla-like structured nanoparticles placed inside silica mesopores have first been prepared on the commercial meso-macroporous silica carrier with a low surface area and were tested in TNB reduction with hydrogen at mild conditions. Catalysts with a Cu loading of 9–15 wt% are first shown to possess high catalytic activity at 170 °C and the initial H₂ pressure of 1.3 MPa that makes it possible to transform trinitrobenzene to amines as major products in organic solutions (concentration 13 g/L) in a matter of 1–2 h at a large mass ratio TNB:catalyst = 2:1. We have successfully performed the hydrogenation of trinitrobenzene on the catalysts based on the Cu₂Si₂O₅(OH)₂/SiO₂ materials that were only calcined preliminarily at 300 or 600 °C. *in situ* reduction in a reaction mixture seems more preferable than any separate reduction step, especially for an industrial process, as well as for the handling and storage of catalysts bearing so easily oxidized Cu nanoparticles.

The presented results bring to engineering and scientific society the potential of Cu phyllosilicate catalysts for the utilization of trinitroaromatic compounds via chemical reduction with catalytic hydrogenation to valuable amines in a batch mode system. Moreover, the catalyst can be used 2–3 times after separation from a reaction mixture. Taking into account the obtained results and the low cost of the prepared Cu₂Si₂O₅(OH)₂/SiO₂ catalytic material, its application for a remediation treatment system, which is based on combining

adsorption and chemical reduction technologies, makes sense to be considered and studied more precisely at a later time.

Supplementary Materials: The following supporting information can be downloaded at: <https://www.mdpi.com/article/10.3390/catal14100686/s1>, Figure S1. XRD patterns of the initial dried material (a) and the materials calcined at 300 °C (b); Figure S2. N₂ adsorption–desorption isotherms; Figure S3. N₂ adsorption isotherms of high resolution; Figure S4. Dependence of the TNB conversion (X) and selectivity to individual amines (Si) versus reaction time for the samples with a Cu loading 6.0 wt.% dried (a) and calcined at 300 °C (b). Samples prepared on the commercial silica with SBET = 300 m²g^{−1}; Table S1. Results of recycling tests of synthesized material (calcined 3Cu-300).

Author Contributions: Conceptualization, O.A.K. and L.M.K.; methodology, E.V.S.; validation, G.I.K., N.A.D. and I.V.M.; investigation, O.A.K. and E.V.S.; writing—original draft preparation, O.A.K.; writing—review and editing, L.M.K.; supervision, L.M.K.; project administration, L.M.K.; funding acquisition, L.M.K. All authors have read and agreed to the published version of the manuscript.

Funding: The research was financially supported by Russian Science Foundation (grant no. 23-73-30007).

Data Availability Statement: Data are available upon request.

Acknowledgments: Electron microscopy characterization was performed in the Department of Structural Studies of Zelinsky Institute of Organic Chemistry, Moscow.

Conflicts of Interest: The authors declare no conflicts of interest.

References

1. Busca, G.; Spennati, E.; Riani, P.; Garbarino, G. Mechanistic and Compositional Aspects of Industrial Catalysts for Selective CO₂ Hydrogenation Processes. *Catalysts* **2024**, *14*, 95. [CrossRef]
2. Bian, Z.; Zhong, W.; Yu, Y.; Jiang, B.; Kawi, S. Cu/SiO₂ derived from copper phyllosilicate for low-temperature water-gas shift reaction: Role of Cu⁺ sites. *Int. J. Hydrogen Energy* **2020**, *45*, 27078–27088. [CrossRef]
3. Mao, M.; Liu, L.; Liu, Z. Recent Insights into Cu-Based Catalytic Sites for the Direct Conversion of Methane to Methanol. *Molecules* **2022**, *27*, 7146. [CrossRef] [PubMed]
4. Ye, R.; Xiao, S.; Lai, Q.; Wang, D.; Huang, Y.; Feng, G.; Zhang, R.; Wang, T. Advances in Enhancing the Stability of Cu-Based Catalysts for Methanol Reforming. *Catalysts* **2022**, *12*, 747. [CrossRef]
5. Zhang, H.; Tan, H.-R.; Jaenicke, S.; Chuah, G.-K. Highly efficient and robust Cu catalyst for non-oxidative dehydrogenation of ethanol to acetaldehyde and hydrogen. *J. Catal.* **2020**, *389*, 19–28. [CrossRef]
6. Averin, A.D.; Panchenko, S.P.; Murashkina, A.V.; Fomenko, V.I.; Kuliukhina, D.S.; Malysheva, A.S.; Yakushev, A.A.; Abel, A.S.; Beletskaya, I.P. Recent Achievements in the Copper-Catalyzed Arylation of Adamantane-Containing Amines, Di- and Polyamines. *Catalysts* **2023**, *13*, 831. [CrossRef]
7. Zhu, Y.; Kong, X.; Peng, B.; Li, L.; Fang, Z.; Zhu, Y. Efficient Cu catalyst for 5-hydroxymethylfurfural hydrogenolysis by forming Cu–O–Si bonds. *Catal. Sci. Technol.* **2020**, *10*, 7323–7330. [CrossRef]
8. Simakova, I.; Demidova, Y.; Simonov, M.; Prikhod'ko, S.; Niphadkar, P.; Bokade, V.; Dhepe, P.; Murzin, D.Y. Heterogeneously Catalyzed γ -Valerolactone Hydrogenation into 1,4-Pentanediol in Milder Reaction Conditions. *Reactions* **2020**, *1*, 54–71. [CrossRef]
9. To, D.-T.; Lin, Y.-C. Copper Phyllosilicates-Derived Catalysts in the Production of Alcohols from Hydrogenation of Carboxylates, Carboxylic Acids, Carbonates, Formyls, and CO₂: A Review. *Catalysts* **2021**, *11*, 255. [CrossRef]
10. Redina, E.; Tkachenko, O.; Salmi, T. Recent Advances in C₅ and C₆ Sugar Alcohol Synthesis by Hydrogenation of Monosaccharides and Cellulose Hydrolytic Hydrogenation over Non-Noble Metal Catalysts. *Molecules* **2022**, *27*, 1353. [CrossRef]
11. Wu, J.; Liu, G.; Liu, Q.; Zhang, Y.; Ding, F.; Wang, K. A Cu-SiO₂ Catalyst for Highly Efficient Hydrogenation of Methyl Formate to Methanol. *Catalysts* **2023**, *13*, 1038. [CrossRef]
12. Boddula, R.; Shanmugam, P.; Srivatsava, R.K.; Tabassum, N.; Pothu, R.; Naik, R.; Saran, A.; Viswanadham, B.; Radwan, A.B.; Al-Qahtani, N. Catalytic Valorisation of Biomass-Derived Levulinic Acid to Biofuel Additive—Valerolactone: Influence of Copper Loading on Silica Support. *Reactions* **2023**, *4*, 465–477. [CrossRef]
13. Ren, X.; Zhou, M.; Yu, W.; Zheng, M.; An, Q. Catalytic Hydrogenation of γ -Butyrolactone to Butanediol over a High-Performance Cu-SiO₂ Catalyst. *Catalysts* **2024**, *14*, 297. [CrossRef]
14. Guo, K.; Wang, W.; Ye, Y.; Chen, L.; Wang, L.; Wang, J.; Zhu, J. Dehydrogenation of Diethylene Glycol to Para-Dioxanone over Cu/SiO₂ Catalyst: Effect of Structural and Surface Properties. *Catalysts* **2024**, *14*, 20. [CrossRef]
15. García-Sancho, C.; Mérida-Robles, J.M.; Cecilia-Buenestado, J.A.; Moreno-Tost, R.; Maireles-Torres, P.J. The Role of Copper in the Hydrogenation of Furfural and Levulinic Acid. *Int. J. Mol. Sci.* **2023**, *24*, 2443. [CrossRef]

16. Cavuoto, D.; Ardemani, L.; Ravasio, N.; Zaccheria, F.; Scotti, N. Some Insights into the Use of Heterogeneous Copper Catalysts in the Hydroprocessing of Levulinic Acid. *Catalysts* **2023**, *13*, 697. [[CrossRef](#)]
17. Zhang, R.; Zhang, J.; Liu, H.; Jiang, Z.; Liu, X.; Wang, W.; Peng, L.; Hu, C. Toward Value-Added Chemicals from Carbohydrates via C–C Bond Cleavage and Coupling Transformations. *ACS Catal.* **2024**, *14*, 5167–5197. [[CrossRef](#)]
18. Formenti, D.; Ferretti, F.; Scharnag, F.K.; Beller, M. Reduction of nitro compounds using 3d-non-noble metal catalysts. *Chem. Rev.* **2019**, *119*, 2611. [[CrossRef](#)]
19. Song, J.; Huang, Z.-F.; Pan, L.; Li, K.; Zhang, X.; Wang, L.; Zou, J.-J. Review on selective hydrogenation of nitroarene by catalytic, photocatalytic and electrocatalytic reactions. *Appl. Catal. B Environ.* **2018**, *227*, 386–408. [[CrossRef](#)]
20. Hu, Z.-N.; Liang, J.; Ding, K.; Ai, Y.; Liang, Q.; Sun, H.-B. Insight into the selectivity of nano-catalytic nitroarenes reduction over other active groups by exploring hydrogen sources and metal components. *Appl. Catal. A Gen.* **2021**, *626*, 118339. [[CrossRef](#)]
21. Kadam, H.K.; Tilve, S.G. Advancement in methodologies for reduction of Nitroarenes. *RSC Adv.* **2015**, *5*, 83391. [[CrossRef](#)]
22. Zeynizadeh, B.; Aminzadeh, F.M.; Mousavi, H. Chemoselective reduction of nitroarenes, N-acetylation of arylamines, and one-pot reductive acetylation of nitroarenes using carbon-supported palladium catalytic system in water. *Res. Chem. Intermed.* **2021**, *47*, 3289–3312. [[CrossRef](#)]
23. Mironenko, R.M.; Belskaya, O.B.; Stepanova, L.N.; Gulyaeva, T.I.; Trenikhin, M.V.; Likholobov, V.A. Palladium Supported on Carbon Nanoglobules as a Promising Catalyst for Selective Hydrogenation of Nitroarenes. *Catal. Lett.* **2020**, *150*, 888–900. [[CrossRef](#)]
24. Bilal, M.; Bagheri, A.R.; Bhatt, P.; Chen, S. Environmental occurrence, toxicity concerns, and remediation of recalcitrant nitroaromatic compounds. *J. Environ. Manag.* **2021**, *291*, 112685. [[CrossRef](#)] [[PubMed](#)]
25. Tiwari, J.; Tarale, P.; Sivanesan, S.; Bafana, A. Environmental persistence, hazard, and mitigation challenges of nitroaromatic compounds. *Environ. Sci. Pollut. Res.* **2019**, *26*, 28650–28667. [[CrossRef](#)] [[PubMed](#)]
26. Niakan, M.; Masteri-Farahani, M. Ultrafine and well-dispersed Pd-Ni bimetallic catalyst stabilized by dendrimer-grafted magnetic graphene oxide for selective reduction of toxic nitroarenes under mild conditions. *J. Hazard. Mater.* **2022**, *424*, 127717. [[CrossRef](#)]
27. Budi, C.S.; Deka, J.R.; Hsu, W.C.; Saikia, D.S.; Chen, K.T.; Kao, H.M.; Yang, Y.C. Bimetallic Co/Zn zeolitic imidazolate framework ZIF-67 supported Cu nanoparticles: An excellent catalyst for reduction of synthetic dyes and nitroarenes. *J. Hazard. Mater.* **2021**, *40*, 124392. [[CrossRef](#)]
28. Zhu, Q.; Zhang, Y.; Zhou, F.; Lv, F.; Ye, Z.; Fan, F.; Chu, P.K. Preparation and characterization of Cu₂O–ZnO immobilized on diatomite for photocatalytic treatment of red water produced from manufacturing of TNT. *Chem. Eng. J.* **2011**, *171*, 61–68. [[CrossRef](#)]
29. Wu, S.; Qi, Y.; He, S.; Fan, C.; Dai, B.; Zhou, W.; Gao, L.; Huang, J. Preparation and application of novel catalytic-ceramic-filler in a coupled system for TNT manufacturing wastewater treatment. *Chem. Eng. J.* **2015**, *280*, 417–425. [[CrossRef](#)]
30. Qin, L.; Zeng, G.; Lai, C.; Huang, D.; Zhang, C.; Cheng, M.; Yi, H.; Liu, X.; Zhou, C.; Xiong, W.; et al. Synthetic strategies and application of gold-based nanocatalysts for nitroaromatics reduction. *Sci. Total Environ.* **2019**, *652*, 93–116. [[CrossRef](#)]
31. Zhao, J.X.; Chen, C.Q.; Xing, C.H.; Jiao, Z.F.; Yu, M.T.; Mei, B.B.; Yang, J.; Zhang, B.Y.; Jiang, Z.; Qin, Y. Selectivity regulation in Au-catalyzed nitroaromatic hydrogenation by anchoring single-site metal oxide promoters. *ACS Catal.* **2020**, *10*, 2837–2844. [[CrossRef](#)]
32. Lara, P.; Philippot, K. The hydrogenation of nitroarenes mediated by platinum nanoparticles: An overview. *Catal. Sci. Technol.* **2014**, *4*, 2445–2465. [[CrossRef](#)]
33. Kottappara, R.; Pillai, S.C.; Vijayan, B.K. Copper-based nanocatalysts for nitroarene reduction—A review of recent advances. *Inorg. Chem. Commun.* **2020**, *121*, 108181. [[CrossRef](#)]
34. Niu, H.; Lu, J.; Song, J.; Pan, L.; Zhang, X.; Wang, L.; Zou, J.-J. Iron Oxide as a Catalyst for Nitroarene Hydrogenation: Important Role of Oxygen Vacancies. *Ind. Eng. Chem. Res.* **2016**, *55*, 8527–8533. [[CrossRef](#)]
35. Miyazaki, M.; Ariyama, K.; Furukawa, S.; Takayama, T.; Komatsu, T. Chemoselective Hydrogenation of Nitroarenes Using Ni–Fe Alloy Catalysts at Ambient Pressure. *ChemistrySelect* **2021**, *6*, 5538–5544. [[CrossRef](#)]
36. Nandi, S.; Patel, P.; Khan, N.H.; Biradar, A.V.; Kureshy, R.I. Nitrogen-rich graphitic-carbon stabilized cobalt nanoparticles for chemoselective hydrogenation of nitroarenes at milder conditions. *Inorg. Chem. Front.* **2018**, *5*, 806–813. [[CrossRef](#)]
37. Wei, X.; Zhou, M.; Zhang, X.; Wang, X.; Wu, Z. Amphiphilic Mesoporous Sandwich-Structured Catalysts for Selective Hydrogenation of 4-Nitrostyrene in Water. *ACS Appl. Mater. Interfaces* **2019**, *11*, 39116–39124. [[CrossRef](#)]
38. Sheng, Y.; Lin, X.; Yue, S.; Liu, Y.; Zou, X.; Wang, X.; Lu, X. Highly efficient non-noble metallic NiCu nanoalloy catalysts for hydrogenation of nitroarenes. *Mater. Adv.* **2021**, *2*, 6722–6730. [[CrossRef](#)]
39. He, D.; Wang, T.; Li, T.; Wang, X.; Wang, H.; Dai, X.; Shi, F. Efficient hydrogenation catalyst designing via preferential adsorption sites construction towards active copper. *J. Catal.* **2021**, *400*, 397–406. [[CrossRef](#)]
40. Shen, M.Q.; Liu, H.; Yu, C.; Yin, Z.Y.; Muzzio, M.; Li, J.R.; Xi, Z.; Yu, Y.S.; Sun, S.H. Room-temperature chemoselective reduction of 3-nitrostyrene to 3-vinylaniline by ammonia borane over Cu nanoparticles. *J. Am. Chem. Soc.* **2018**, *140*, 16460–16463. [[CrossRef](#)]
41. Ma, Z.H.; Liu, H.; Yue, M. Magnetically recyclable Sm₂Co₁₇/Cu catalyst to chemoselectively reduce the 3-nitrostyrene into 3-vinylaniline under room temperature. *Nano Res.* **2019**, *12*, 3085–3088. [[CrossRef](#)]
42. Zhao, Y.; Li, S.; Wang, Y.; Shan, B.; Zhang, J.; Wang, S.; Ma, X. Efficient tuning of surface copper species of Cu/SiO₂ catalyst for hydrogenation of dimethyl oxalate to ethylene glycol. *Chem. Eng. J.* **2017**, *313*, 759. [[CrossRef](#)]

43. Xu, C.; Chen, G.; Zhao, Y.; Liu, P.; Duan, X.; Gu, L.; Fu, G.; Yuan, Y.; Zheng, N. Interfacing with silica boosts the catalysis of copper. *Nat. Commun.* **2018**, *9*, 3367. [[CrossRef](#)] [[PubMed](#)]
44. Zhu, W.; Sun, P.; Ran, W.; Zheng, Y.; Wang, L.; Zhang, L.; Jia, X.; Chen, J.; Wang, J.; Zhang, H.; et al. Rational design and facile hydrothermal-thermal conversion synthesis of hierarchical porous urchin-like $\text{Cu}_{2x}\text{Si}_2\text{O}_5(\text{OH})_3 \cdot x\text{H}_2\text{O}$ and CuO/SiO_2 hollow microspheres for high efficiency catalytic reduction of nitroarenes and adsorption of organic dye. *Chem. Eng. J.* **2021**, *411*, 128442. [[CrossRef](#)]
45. Zhang, X.-Q.; Shen, R.-F.; Guo, X.-J.; Yan, X.; Chen, Y.; Hu, J.-T.; Lang, W.-Z. Bimetallic Ag-Cu nanoparticles anchored on polypropylene (PP) nonwoven fabrics: Superb catalytic efficiency and stability in 4-nitrophenol reduction. *Chem. Eng. J.* **2021**, *408*, 128018. [[CrossRef](#)]
46. Feng, Y.; Wang, A.; Yin, H.; Yan, X.; Shen, L. Reduction of 3-nitro-4-methoxy-acetylaniline to 3-amino-4-methoxyacetylaniline catalyzed by metallic Cu nanoparticles at low reaction temperature. *Chem. Eng. J.* **2015**, *262*, 427–435. [[CrossRef](#)]
47. Rajendran, K.; Pandurangan, N.; Vinod, C.P.; Khan, T.S.; Gupta, S.; Haider, M.A.; Jagadeesan, D. CuO as a reactive and reusable reagent for the hydrogenation of nitroarenes. *Appl. Catal. B Environ.* **2021**, *297*, 120417. [[CrossRef](#)]
48. Li, M.; Hao, Y.; Cárdenas-Lizana, F.; Yiu, H.H.P.; Keane, M.A. Hydrogen-Free Hydrogenation of Nitrobenzene Over Cu/SiO_2 Via Coupling with 2-Butanol Dehydrogenation. *Top. Catal.* **2015**, *58*, 149–158. [[CrossRef](#)]
49. Li, W.; Cui, X.; Junge, K.; Surkus, A.E.; Kreyenschulte, C.; Bartling, S.; Beller, M. General and chemoselective copper oxide catalysts for hydrogenation reactions. *ACS Catal.* **2019**, *9*, 4302–4307. [[CrossRef](#)]
50. Shuvalova, E.V.; Kirichenko, O.A.; Kapustin, G.I.; Kustov, L.M. Silica-supported copper nanoparticles as efficient catalysts for the liquid-phase selective hydrogenation of p-dinitrobenzene by molecular hydrogen. *Russ. Chem. Bull.* **2016**, *65*, 2850–2854. [[CrossRef](#)]
51. Shuvalova, E.V.; Kirichenko, O.A. Hydrogenation of nitroarenes on silica-supported copper catalyst. *Mendeleev Commun.* **2021**, *31*, 875–877. [[CrossRef](#)]
52. Chatterjee, S.; Deb, U.; Datta, S.; Walther, C.; Gupta, D.K. Common explosives (TNT, RDX, HMX) and their fate in the environment: Emphasizing bioremediation. *Chemosphere* **2017**, *184*, 438–451. [[CrossRef](#)] [[PubMed](#)]
53. Hawari, J.; Halasz, A.; Beaudet, S.; Paquet, L.; Ampleman, G.; Thiboutot, S. Biotransformation of 2,4,6-TNT by phanerochaete chrysosporium in agitated cultures at pH 4.5. *Appl. Environ. Microbiol.* **1999**, *65*, 2977–2986. [[CrossRef](#)] [[PubMed](#)]
54. Rodgers, J.D.; Bunce, N.J. Treatment Methods for the Remediation of Nitroaromatic Explosives. *Water Res.* **2001**, *35*, 2101–2111. [[CrossRef](#)]
55. Liou, M.-J.; Lu, M.-C. Catalytic degradation of nitroaromatic explosives with Fenton's reagent. *J. Mol. Catal. A Chem.* **2007**, *277*, 155–163. [[CrossRef](#)]
56. Zhang, Q.; Meng, Z.; Zhang, Y.; Lv, G.; Lv, F.; Wu, L. Modification of a Na-montmorillonite with quaternary ammonium salts and its application for organics removal from TNT red water. *Water Sci. Technol.* **2014**, *69*, 1798–1804. [[CrossRef](#)]
57. Zhang, C.-L.; Yu, Y.Y.; Fang, Z.; Naraginti, S.; Zhang, Y.; Yong, Y.-C. Recent advances in nitroaromatic pollutants bioreduction by electroactive bacteria. *Process Biochem.* **2018**, *70*, 129–135. [[CrossRef](#)]
58. Madeira, C.L.; Kadoya, W.M.; Li, G.; Wong, S.; Sierra-Alvarez, R.; Field, J.A. Reductive biotransformation as a pretreatment to enhance in situ chemical oxidation of nitroaromatic and nitroheterocyclic explosives. *Chemosphere* **2019**, *222*, 1025–1032. [[CrossRef](#)]
59. Tiwari, J.; Gandhi, D.; Sivanesan, S.; Naoghare, P.; Bafana, A. Remediation of different nitroaromatic pollutants by a promising agent of *Cupriavidus sp.* strain a3. *Ecotoxicol. Environ. Saf.* **2020**, *205*, 111138. [[CrossRef](#)]
60. Bui, D.N.; Minh, T.T. Investigation of TNT red wastewater treatment technology using the combination of advanced oxidation processes. *Sci. Total Environ.* **2021**, *756*, 143852. [[CrossRef](#)]
61. Tartakovsky, V.A.; Shevelev, S.A.; Dutov, M.D.; Shakhnes, A.K.; Rusanov, A.L.; Komarova, L.G.; Andrievsky, A.M. Problems of trotyl (TNT) processing into condensation monomers, polymers and dyes. In *Conversion Concepts for Commercial Applications and Disposal Technologies of Energetic Systems*; Krause, H., Ed.; Kluwer Academic Publishers: Dordrecht, The Netherlands, 1997; pp. 37–149.
62. Belskaya, O.B.; Mironenko, R.M.; Talsi, V.P.; Rodionov, V.A.; Sysolyatin, S.V.; Likhobobov, V.A. A study of Pd/C catalysts in the liquid-phase hydrogenation of 1,3,5-trinitrobenzene and 2,4,6-trinitrobenzoic acid. Selection of hydrogenation conditions for selective production of 1,3,5-Triaminobenzene. *Procedia Eng.* **2016**, *152*, 110–115. [[CrossRef](#)]
63. Belskaya, O.B.; Mironenko, R.M.; Talsi, V.P.; Rodionov, V.A.; Gulyaeva, T.A.; Sysolyatin, S.V.; Likhobobov, V.A. The effect of preparation conditions of Pd/C catalyst on its activity and selectivity in the aqueous-phase hydrogenation of 2,4,6-trinitrobenzoic acid. *Catal. Today* **2018**, *301*, 258–265. [[CrossRef](#)]
64. Shchurova, I.A.; Arbagozova, A.A.; Alekseyeva, N.A.; Malykhin, V.V. Catalytic Hydrogenation of 1,3,5-Trinitrobenzene. *Yuzhno Sib. Nauchn. Vestn.* **2019**, *28*, 166–170. (In Russian) [[CrossRef](#)]
65. Shchurova, I.A.; Alekseyeva, N.A.; Sysolyatin, S.V.; Malykhin, V.V. A Comparative Study of the Synthesis and Hydrolysis of sym-Triaminobenzene Homologues. *Molecules* **2022**, *27*, 8595. [[CrossRef](#)]
66. Belskaya, O.B.; Talsi, V.P.; Mironenko, R.M.; Rodionov, V.A.; Sysolyatin, S.V.; Likhobobov, V.A. Transformation pathways of 2,4,6-trinitrobenzoic acid in the aqueous-phase hydrogenation over Pd/C catalyst. *J. Mol. Catal. A Chem.* **2016**, *420*, 190–199. [[CrossRef](#)]

67. Mironenko, R.M.; Belskaya, O.B.; Talsi, V.P.; Rodionov, V.A.; Sysolyatin, S.V.; Likholobov, V.A. An unusual reduction route of 2,4,6-trinitrobenzoic acid under conditions of aqueous-phase hydrogenation over Pd/Sibunit catalyst. *Russ. Chem. Bull.* **2016**, *65*, 1535–1540. [[CrossRef](#)]
68. Neri, G.; Musolino, M.G.; Bonaccorsi, M.G.; Donato, L.; Mercadante, L. Catalytic hydrogenation of 4-(hydroxyamino)-2-nitrotoluene and 2,4-nitroamine isomers. *Ind. Eng. Chem. Res.* **1997**, *36*, 3619–3624. [[CrossRef](#)]
69. Chernyshev, V.M.; Khazipov, O.V.; Eremin, D.B.; Denisova, E.A.; Ananikov, V.P. Formation and stabilization of nanosized Pd particles in catalytic systems: Ionic nitrogen compounds as catalytic promoters and stabilizers of nanoparticles. *Coord. Chem. Rev.* **2021**, *437*, 213860. [[CrossRef](#)]
70. Nuzhdin, A.L.; Shchurova, I.A.; Bukhtiyarova, M.V.; Bulavchenko, O.A.; Alekseyeva, N.A.; Sysolyatin, S.V.; Bukhtiyarova, G.A. Flow Hydrogenation of 1,3,5-Trinitrobenzenes over Cu-Based Catalysts as an Efficient Approach for the Preparation of Phloroglucinol Derivatives. *Synthesis* **2022**, *54*, 3605–3612. [[CrossRef](#)]
71. Nuzhdin, A.L.; Shchurova, I.A.; Bukhtiyarova, M.V.; Plyusnin, P.E.; Alekseyeva, N.A.; Sysolyatin, S.V.; Bukhtiyarova, G.A. Comparative Study of the Hydrogenation of 1,3,5-Trinitrobenzene and 2,4,6-Trinitrotoluene over a Copper–Alumina Catalyst in a Flow Reactor. *Kinet. Catal.* **2023**, *64*, 25–31. [[CrossRef](#)]
72. Rathi, B.S.; Kumar, P.S.; Vo, D.-V.N. Critical review on hazardous pollutants in water environment: Occurrence, monitoring, fate, removal technologies and risk assessment. *Sci. Total Environ.* **2021**, *797*, 149134. [[CrossRef](#)] [[PubMed](#)]
73. Hariu, T.; Arima, H.; Sugiyama, K. The structure of hydrated copper-silicate gels, an analog compound for natural chrysocolla. *J. Miner. Petrol. Sci.* **2013**, *108*, 111–115. [[CrossRef](#)]
74. Kirichenko, O.; Kapustin, G.; Mishin, I.; Nissenbaum, V.; Shuvalova, E.; Redina, E.; Kustov, L. Facile synthesis of micro-mesoporous copper phyllosilicate supported on a commercial carrier and its application for catalytic hydrogenation of nitro-group in trinitrobenzene. *Molecules* **2022**, *27*, 5147. [[CrossRef](#)] [[PubMed](#)]
75. Kirichenko, O.A.; Shuvalova, E.V.; Strekalova, A.A.; Davshan, N.A.; Kapustin, G.I.; Nissenbaum, V.D. Catalytic activity of Cu and Cu–Fe hydrosilicates in hydrogenation with molecular hydrogen. *Russ. J. Phys. Chem.* **2018**, *92*, 2417–2423. [[CrossRef](#)]
76. Kirichenko, O.A.; Shuvalova, E.V.; Redina, E.A. Low-temperature copper hydrosilicates: Catalysts for reduction of aromatic nitro compounds with molecular hydrogen. *Russ. Chem. Bull.* **2019**, *68*, 2048–2052. [[CrossRef](#)]
77. Di, W.; Cheng, J.; Tian, S.; Li, J.; Chen, J.; Sun, Q. Synthesis and characterization of supported copper phyllosilicate catalysts for acetic ester hydrogenation to ethanol. *Appl. Catal. A Gen.* **2016**, *510*, 244–259. [[CrossRef](#)]
78. Van der Grift, C.J.G.; Wielers, A.F.H.; Mulder, A.; Geus, J.W. The reduction behavior of silica-supported copper catalysts prepared by deposition-precipitation. *Thermochim. Acta* **1990**, *171*, 95–113. [[CrossRef](#)]
79. Zhang, J.; Ding, G.; Jin, Y.; Wei, L.; Li, X.; Wang, D.; Zhu, Y.; Li, Y. Stabilizing the interfacial Cu⁰-Cu⁺ dual sites toward furfural hydrodeoxygenation to 2-methylfuran via fabricating nest-like copper phyllosilicate precursor. *Fuel* **2022**, *337*, 127212. [[CrossRef](#)]
80. Toupance, T.; Kermarec, M.; Lambert, J.-F.; Louis, C. Conditions of formation of copper phyllosilicates in silica-supported copper catalysts prepared by selective adsorption. *J. Phys. Chem. B* **2002**, *106*, 2277–2286. [[CrossRef](#)]
81. Talsi, V.P.; Belskaya, O.B.; Yurpalov, V.L. The composition of transformation products of 2,4,6-trinitrobenzoic acid in the aqueous-phase hydrogenation over Pd/C catalysts. *Magn. Reson. Chem.* **2020**, *58*, 84–96. [[CrossRef](#)]
82. Blaser, H.-U.; Steiner, H.; Studer, M. Selective catalytic hydrogenation of functionalized nitroarenes: An update. *ChemCatChem* **2009**, *1*, 210–221. [[CrossRef](#)]
83. Thommes, M.; Kaneko, K.; Neimark, A.V.; Olivier, J.P.; Rodriguez-Reinoso, F.; Rouquerol, J.; Sing, K.S.W. Physisorption of gases, with special reference to the evaluation of surface area and pore size distribution (IUPAC Technical Report). *Pure Appl. Chem.* **2015**, *87*, 1051–1069. [[CrossRef](#)]
84. Neimark, A.V.; Sing, K.S.W.; Thommes, M. Characterization of solid catalysts: Surface area and porosity. In *Handbook of Heterogeneous Catalysis*; Ertl, G., Knozinger, H., Schuth, F., Weitkamp, J., Eds.; Wiley-VCH Verlag GmbH & Co. KGaA: Weinheim, Germany, 2008; pp. 721–729.
85. Greg, S.J.; Sing, K.S.W. *Adsorption, Surface Area and Porosity*, 2nd ed.; Academic Press: London, UK, 1982.
86. Van der Grift, C.J.G.; Elberse, P.A.; Mulder, A.; Geus, J.W. Preparation of silica-supported copper catalysts by means of deposition precipitation. *Appl. Catal.* **1990**, *59*, 275–289. [[CrossRef](#)]
87. Redina, E.; Arkhipova, N.; Kapustin, G.; Kirichenko, O.; Mishin, I.; Kustov, L. Ceria-Modified Copper Phyllosilicate Catalyst for One-Pot Hydroamination of 5-HMF with Nitro-Compounds. *ChemCatChem* **2023**, *15*, e202300294. [[CrossRef](#)]

Disclaimer/Publisher’s Note: The statements, opinions and data contained in all publications are solely those of the individual author(s) and contributor(s) and not of MDPI and/or the editor(s). MDPI and/or the editor(s) disclaim responsibility for any injury to people or property resulting from any ideas, methods, instructions or products referred to in the content.